Heliyon 9 (2023) e15882

Contents lists available at ScienceDirect

# Heliyon

journal homepage: www.cell.com/heliyon

Research article

# Investigation of space division multiplexing in multimode step-index silica photonic crystal fibers

Svetislav Savović [a], Konstantinos Aidinis [b,c], Alexandar Djordjevich [d], Rui Min [e,*]

[a] University of Kragujevac, Faculty of Science, R. Domanovića 12, 34000 Kragujevac, Serbia
[b] Department of Electrical Engineering, Ajman University, P.O. Box 346, Ajman, United Arab Emirates
[c] Center of Medical and Bio-allied Health Sciences Research, Ajman University, P. O. Box 346, Ajman, United Arab Emirates
[d] City University of Hong Kong, 83 Tat Chee Avenue, Kowloon, Hong Kong, China
[e] Center for Cognition and Neuroergonomics, State Key Laboratory of Cognitive Neuroscience and Learning, Beijing Normal University, Zhuhai 519087, China

ARTICLE INFO

*Keywords:*
Photonic crystal fiber
Space division multiplexing
Power flow equation

ABSTRACT

The feasible distance is presented for space division multiplexed (SDM) transmission along multimode silica step-index photonic crystal fiber (SI PCF) by solving the time-independent power flow equation (TI PFE). These distances for two and three spatially multiplexed channels were determined to depend on mode coupling, fiber structural parameters, and launch beam width in order to keep crosstalk in two- and three-channel modulation to a maximum of 20% of the peak signal strength. We found that the length of the fiber at which an SDM can be realized increases with the size of the air-holes in the cladding (higher NA). When a wide launch excites more guiding modes, these lengths become shorter. Such knowledge is valuable for the use of multimode silica SI PCFs in communications.

## 1. Introduction

An increase of optical fiber networks capacity is being driven by the demand for more data bandwidth. Multiplexing of optical data in space, time, polarization, wavelength and phase, may be able to address the strong demand for capacity growth. Both high-power and low-power fiber optics systems can use multiplexing [1,2]. SDM is a technology that allows multiple optical signals to be transmitted over separate spatial paths within a single-core or multicore fibers. The modes which are transmitted over these separate spatial paths are used to transmit separate data streams within the fiber, effectively increasing the capacity of the fiber. In each of these approaches, the individual modes within the fiber have to be carefully controlled and manipulated to ensure that they can be used to transmit data effectively. One of the key advantages of SDM fiber optic systems is that they can provide a significant increase in capacity without the need for additional fibers or complex network infrastructure. This can help to reduce costs and simplify network management, making it easier to deploy and maintain high-speed communication networks. In the past ten years, SDM has received a lot of interest for the capacity development in fiber optics communications [1–8]. Each SDM channel in the case of SDM is given a radially distributed spatial location inside the fiber. The incident angle and strength of coupling between a propagating modes define the position of each channel within the fiber. While all subsequent channels characterized with an incident angle of $\theta_0 > 0^\circ$ seem as concentric rings, the central channel which is with an incident angle of $\theta_0 = 0^\circ$ parallel to the fiber axis actually looks like a disk. The

* Corresponding author.
*E-mail addresses:* rumi@doctor.upv.es, ruimin@bnu.edu.cn (R. Min).

https://doi.org/10.1016/j.heliyon.2023.e15882
Received 17 February 2023; Received in revised form 21 April 2023; Accepted 25 April 2023
Available online 2 May 2023

optical fiber system's bandwidth is increased since each ring and the central disk constitute its own individual spatially modulated optical channel (Fig. 1). However, the intended SDM technique is hampered by random coupling between the channels. With increasing distance from the input end, this interference becomes more and more pronounced. It results from macro- and micro-bending as well as impurities and other flaws that are trapped into the fiber during the production process. Power is transferred between neighboring channels by these irregularities. Referred to as "mode coupling", the outcome is a crosstalk between the SDM channels. With each successive imperfection in the fiber that is encountered, effects spread outward from the input end as more and more of the launch light gets connected to nearby channels. It is unquestionably crucial for the operation of SDM to characterize such performance-limiting effects of mode coupling that result in crosstalk in an SDM scheme. By solving the TI PFE, we accomplish it in this study for the multimode silica SI PCF with a solid-core.

The refractive-index (RI) change in an optical fiber has historically been accomplished by chemical doping. Another method [9,10] includes fabricating a micro-structured pattern of minuscule air-holes in the cladding along the PCFs' length (Fig. 2(a)). Since the air-hole pattern reduces the cladding's effective RI, the fiber can act as a light guide. The RI profile of such a fiber is shown in Fig. 2(b). Commercially available simulation software packages are not adequate for multimode PCFs due to hundreds or even thousands of propagation modes. In this paper, the TI PFE is numerically solved to address this deficiency. In our knowledge for the first time in this work we investigate an SDM capability of multimode silica SI PCF.

## 2. SI PCF design

The SI PCF's cladding is covered with air-holes that are typically homogeneous in size and arranged in a form of triangular lattice. The pitch ($\Lambda$) or the size ($d$) of these air-holes can be changed to get the required effective RI, numerical aperture and dispersion (Fig. 2). Despite having uniform material qualities throughout, the middle part of the fiber without holes has the highest RI $n_0$. Air-holes in the cladding lower this index's effective value $n_1$, and larger or more sparsely distributed air-holes further lower it.

### 2.1. Time-independent power flow equation

We investigate power flow inside the SI PCF using Gloge's TI PFE equation [11]:

$$\frac{\partial P(\theta,z)}{\partial z} = -\alpha(\theta)P(\theta,z) + \frac{D}{\theta}\frac{\partial}{\partial\theta}\left(\theta\frac{\partial P(\theta,z)}{\partial\theta}\right) \tag{1}$$

The term $P(\theta,z)$ is the optical power as a function of the angle of propagation $\theta$ and propagation distance $z$ and $D$ is the coupling coefficient [11–14]. Since mode coupling is unaffected by the modal attenuation, equation (1) reads:

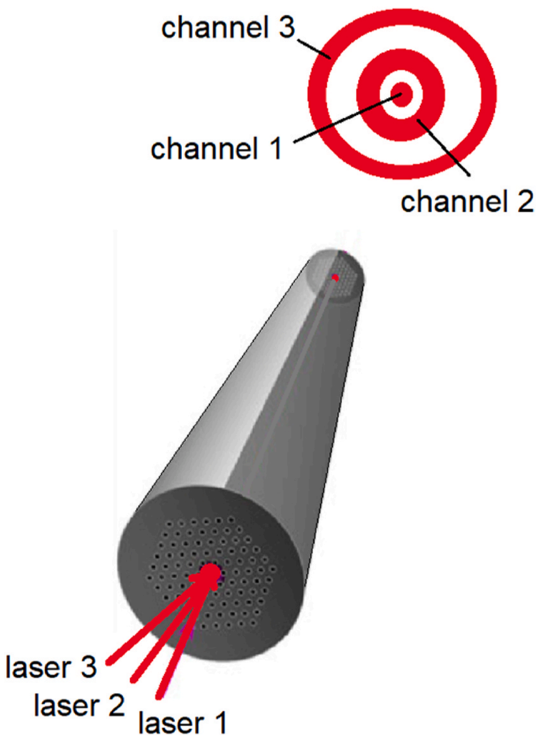


**Fig. 1.** SDM schematics with three channels.

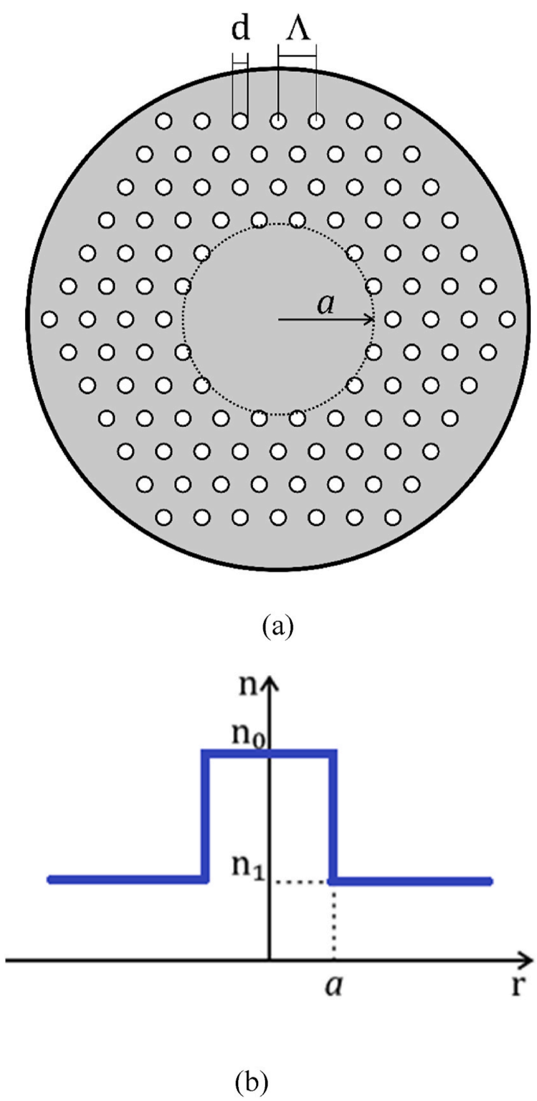


**Fig. 2.** (a) Cross section of multimode SI PCF with a solid-core and rings of air-holes in the cladding, where Λ is the hole-to-hole spacing (pitch), *d* is diameter of air-holes in the cladding. (b) The referent multimode SI PCF's RI profile.

$$\frac{\partial P(\theta,z)}{\partial z}=\frac{D}{\theta}\frac{\partial P(\theta,z)}{\partial \theta}+D\frac{\partial^2 P(\theta,z)}{\partial \theta^2} \tag{2}$$

The explicit finite-difference method (EFDM) is used to solve equation (2) for the optical power $P(\theta,z)$ [14]. At launch, the following Gaussian input power distribution was assumed:

$$P(\theta,z)=\frac{1}{\sigma\sqrt{2\pi}}\exp\left[-\frac{(\theta-\theta_0)^2}{2\sigma^2}\right] \tag{3}$$

where $\theta_0$ is the mean value for the launch angle and $\sigma$ is standard deviation.

## 3. Numerical results

In order to investigate the capacity of SDM for this multimode silica SI PCF, we were able to calculate $P(\theta,z)$ along the fiber by employing the TI PFE. This has been done for various widths of Gaussian input power distributions and cladding's air-hole diameters *d*. For PCFs shown in Fig. 2(a), the effective parameter *V* can be utilized to calculate the effective RI of the cladding $n_{fsm}$:

$$V=\frac{2\pi}{\lambda}a_{eff}\sqrt{n_0^2-n_{fsm}^2} \tag{4}$$

where $n_0$ is the RI of the core, $n_1 \equiv n_{fsm}$ is the effective RI of the cladding and $a_{eff} = \Lambda/\sqrt{3}$ [15]. Using the effective parameter $V$, equation (4) may be used to determine $n_{fsm}$ [15]:

$$V\left(\frac{\lambda}{\Lambda},\frac{d}{\Lambda}\right) = A_1 + \frac{A_2}{1 + A_3\exp(A_4\lambda/\Lambda)} \tag{5}$$

with the fitting parameters $A_i$ ($i = 1$ to 4):

$$A_i = a_{i0} + a_{i1}\left(\frac{d}{\Lambda}\right)^{b_{i1}} + a_{i2}\left(\frac{d}{\Lambda}\right)^{b_{i2}} + a_{i3}\left(\frac{d}{\Lambda}\right)^{b_{i3}} \tag{6}$$

where the coefficients $a_{i0}$ to $a_{i3}$ and $b_{i1}$ to $b_{i3}$ ($i = 1$ to 4) are given in Table 1. The RI $n_{fsm}$, relative RI difference $\Delta$ and critical angles $\theta_m$ for varied air-holes diameter of the cladding $d$, pitch $\Lambda = 3$ μm and λ = 850 nm, are summarized in Table 2.

Using the EFDM [14], we solved the TI PFE (2) for the multimode SI PCF with silica core with $2a = 50$ μm, $n_0 = 1.45$ and $D = 2.3\times 10^{-6}\text{rad}^2/\text{m}$ [16]. In the calculations one can use the same value of $D$ for conventional silica fibers and silica PCF since it is predominantly governed by fiber material. We examined scenarios with $d = 1$ μm and 2 μm and Gaussian incident beams with $(\text{FWHM})_{z=0} = 1$, 3 and 5°. Gaussian beams (3) were launched into multimode silica SI PCF with solid-core with $d = 1$ μm at their respective mean input angles of $\theta_0 = 0$ and 4° (two-channel SDM) and $\theta_0 = 0$, 2 and 4° (three-channel SDM). Gaussian beams were launched into multimode silica SI PCF with $d = 2$ μm at their respective mean input angles of $\theta_0 = 0$ and 8° (two-channel SDM) and $\theta_0 = 0$, 4 and 8° (three-channel SDM). Figs. 3 and 4 demonstrate the normalized power distributions coming from the output fiber-ends in the case of two- and three-channel SDM, respectively, for such input into multimode silica SI PCF with $d = 2$ μm. As seen in Figs. 3(a) and 4(a), where the distributions are essentially unchanged from when the fibers were first launched and exhibit no evidence of signal crosstalk, such distributions remain almost unchanged within the first few tens of meters of fibers. Figs. 3(b) and 4(b) show that with increasing fibers' lengths, coupling between propagating modes results in the broadening of Gaussian distributions. As a result, there is some crosstalk between adjacent co-propagating optical channels because the tails of the various Gaussians overlap to an extent of about 20% of their maxima. In Figs. 3(c) and 4(c), the situation worsens significantly for longer fibers. The rings and the center dot in Fig. 1 that result from these distributions may still be recognizable, but they are severely blurred and morphed close together. This is due to the large crosstalk between neighboring co-propagating optical channels, which is evident as the individual distributions are more difficult to resolve from the overall image. Figs. 3(d) and 4(d) are related to circumstances at "coupling length" $L_c$ (which is the length in a particular fiber at which the highest order launched modes shifted their distributions from ring into disk form). It should come as no surprise that the mode-distributions for the optical channels overlap significantly. The rings and the center dot seen in Fig. 1 are no longer recognizable in the images they produce, which have changed into overlapping disks. In this fiber, three-channel SDM is feasible up to lengths that are significantly shorter than those at which two-channel SDM can be accomplished, with the tolerable mixing threshold of 20% of the maximum intensity being used (Figs. 5 and 6). It should be noticed that these lengths $z_{SDM}$, with the acceptable degree of crosstalk between two and three spatially multiplexed channels, are significantly shorter than the corresponding lengths $L_c$ (Table 3). It is clear that the length $L_c$ increases as the diameter $d$ of air holes increases (increase of NA). This is a result of higher-order modes participating more frequently in higher NA PCFs. We also demonstrate that the length at which EMD is created decreases with increasing launch beam width (Table 3). This is because a wide launch beam drives the EMD at shorter distances than a narrow launch beam does.

It should also be mentioned that in our earlier research, we successfully examined the SDM capabilities in standard multimode SI plastic optical fibers utilizing the TI PFE [17]. In comparison to the multimode silica SI PCF examined in this work, the transmission lengths for space division multiplexing in standard multimode SI plastic optical fibers are significantly shorter. This is dominantly a result of multimode plastic optical fibers having substantially stronger mode coupling than multimode silica optical fibers. For standard plastic optical fibers, a typical value of coupling coefficient is $D \sim 10^{-4}$ rad$^2$/m [14,17]. The results reported in this work could be of great interest not only in fiber optic communication systems but also for various fiber optic sensory systems [18–20]. Finally, it should be mentioned that a similar modeling approach can be used for investigation of bandwidth in each SDM channel.

## 4. Conclusion

The transmission length limit for SDM in multimode silica SI PCF with solid core is investigated using the TI PFE. For the acceptable

**Table 1**
Fitting coefficients in equation (6).

| | $i = 1$ | $i = 2$ | $i = 3$ | $i = 4$ |
|---|---|---|---|---|
| $a_{i0}$ | 0.54808 | 0.71041 | 0.16904 | −1.52736 |
| $a_{i1}$ | 5.00401 | 9.73491 | 1.85765 | 1.06745 |
| $a_{i2}$ | −10.43248 | 47.41496 | 18.96849 | 1.93229 |
| $a_{i3}$ | 8.22992 | −437.50962 | −42.4318 | 3.89 |
| $b_{i1}$ | 5 | 1.8 | 1.7 | −0.84 |
| $b_{i2}$ | 7 | 7.32 | 10 | 1.02 |
| $b_{i3}$ | 9 | 22.8 | 14 | 13.4 |

**Table 2**
Effective RI of the cladding $n_1$ (obtained using equations (5) and (6)), relative RI difference $\Delta = (n_0 - n_1)/n_0$, where $n_0 = 1.45$, and the critical angle $\theta_m$ for varied air-holes diameter $d$ (wavelength: 850 nm).

| $d$ (μm) | 1.0 | 2.0 |
|---|---|---|
| $n_1$ | 1.443717 | 1.423679 |
| $\Delta = (n_0 - n_1)/n_0$ | 0.00433 | 0.01815 |
| $\theta_m$ (deg) | 5.34 | 10.93 |

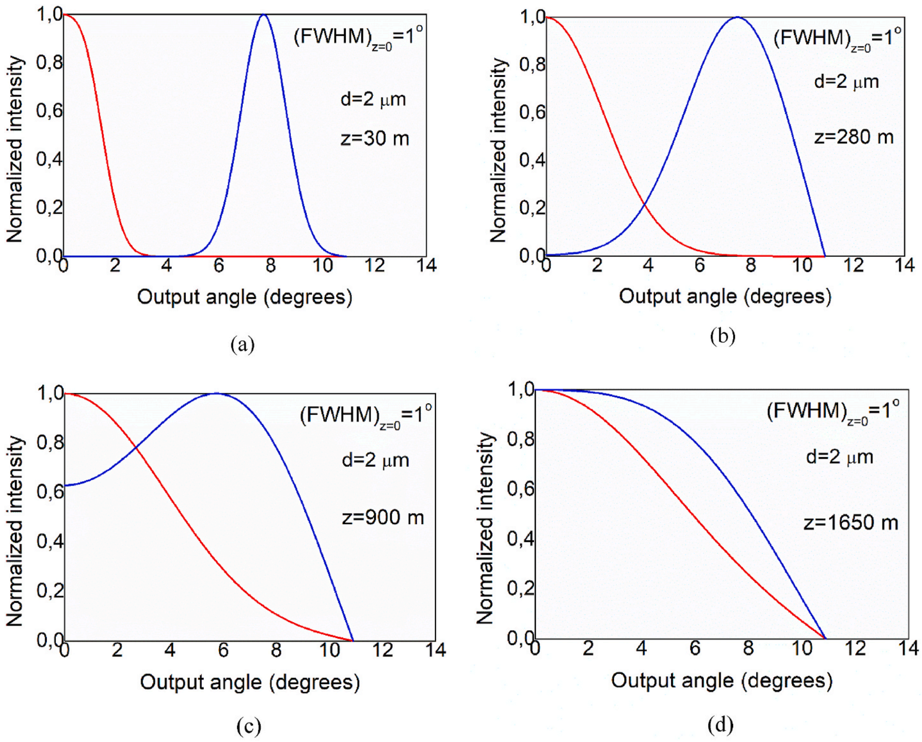


**Fig. 3.** The evolution of the normalized output angular power distribution with fiber length for the case with $d = 2$ μm calculated for two Gaussian beams (two-channel SDM) with input angles $\theta_0 = 0^\circ$ (red line) and 8° (blue line), with $(\mathrm{FWHM})_{z=0} = 1^\circ$ for: (a) $z = 30$ m; (b) $z = 280$ m; (c) $z = 900$ m and (d) $z \equiv L_c = 1650$ m.

crosstalk between 2- and 3-spatially multiplexed channels, these distances were found to be dependent on the strength of mode coupling, the size of the air holes in the cladding and the width of the incident beam. An SDM can be realized at longer lengths because the EMD is established at longer fiber lengths with larger cladding's air-holes. These lengths shorten for a wide launch that stimulates additional guiding modes. As a comparison, the transmission lengths for SDM in multimode plastic optical fibers are significantly shorter. This is dominantly a result of multimode plastic optical fibers having substantially stronger mode coupling than multimode silica optical fibers. When employing a SDM using a multimode silica SI PCFs, results reported in this work should be taken into account.

## Author contribution statement

Svetislav Savović: Conceived and designed the experiments; Performed the experiments; Analyzed and interpreted the data; Contributed reagents, materials, analysis tools or data; Wrote the paper.

Konstantinos Aidinis, Alexandar Djordjevich, and Rui Min: Analyzed and interpreted the data; Contributed reagents, materials, analysis tools or data; Wrote the paper.

## Funding statement

This research was funded by the National Natural Science Foundation of China (62003046, 6211101138); the Strategic Research Grant of City University of Hong Kong (Project No. CityU 7004600) and by a grant from Serbian Ministry of Education, Science and

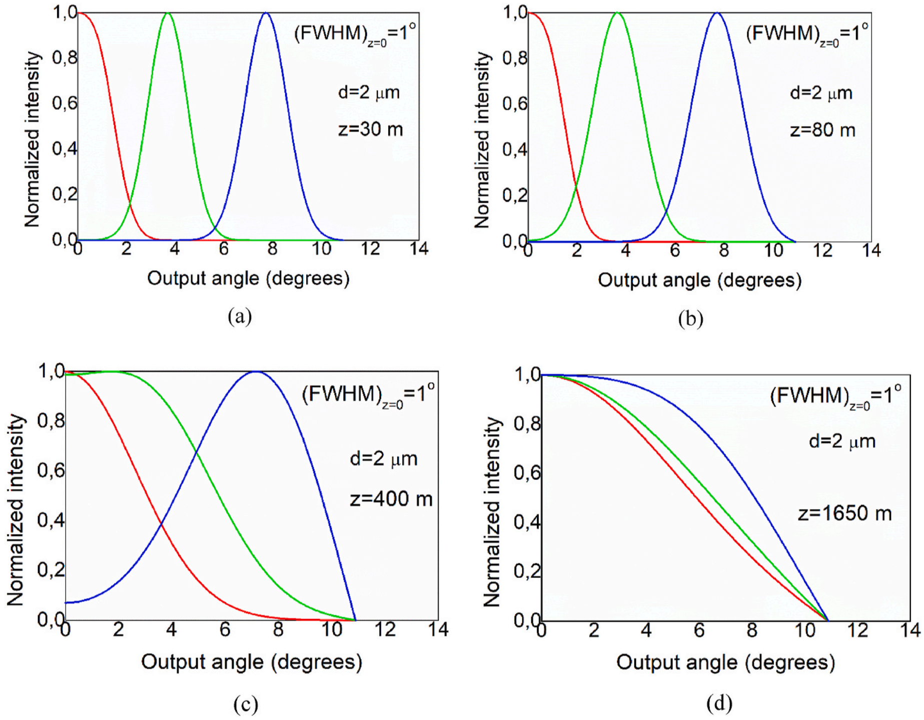


**Fig. 4.** The evolution of the normalized output angular power distribution with fiber length for the case with $d = 2$ μm calculated for three Gaussian beams (three-channel SDM) with input angles $\theta_0 = 0°$ (red line), 4° (green line) and 8° (blue line), with $(FWHM)_{z=0} = 1°$ for: (a) $z = 30$ m; (b) $z = 80$ m; (c) $z = 400$ m and (d) $z \equiv L_c = 1650$ m.

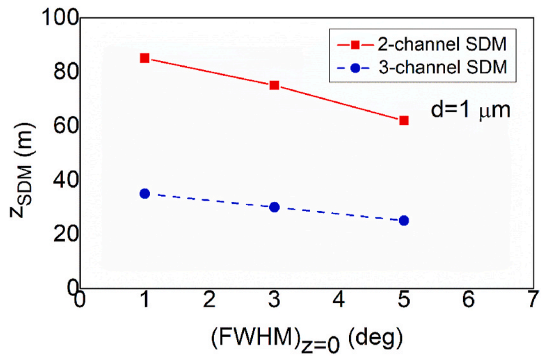


**Fig. 5.** Length $z_{SDM}$ for two and three spatially multiplexed channels with minimal crosstalk in multimode silica SI PCF as a function of $(FWHM)_{z=0}$ of the incident beam, for air-holes diameter in the cladding $d = 1$ μm.

Technological Development (Agreement No. 451-03-68/2022–14/200,122) and by grant from Science Fund of the Republic of Serbia (Agreement No. CTPCF-6379382); Guangdong Basic and Applied Basic Research Foundation (2021A1515011997); Special project in key field of Guangdong Provincial Department of Education (2021ZDZX1050); The Innovation Team Project of Guangdong Provincial Department of Education (2021KCXTD014).

## Data availability statement

Data will be made available on request.

## Additional information

No additional information is available for this paper.

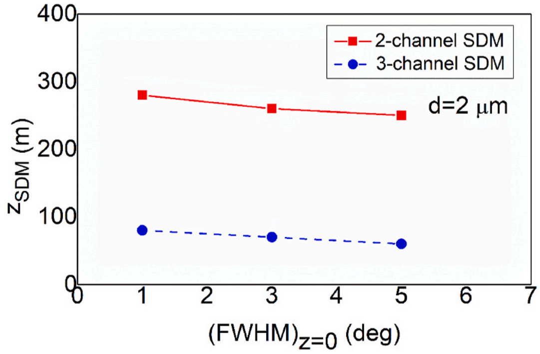


**Fig. 6.** Length $z_{SDM}$ for two and three spatially multiplexed channels with minimal crosstalk in multimode silica SI PCF as a function of $(FWHM)_{z=0}$ of the incident beam, for air-holes diameter in the cladding $d = 2$ μm.

**Table 3**
Minimal crosstalk length $z_{SDM}$ for two and three spatially multiplexed channels and coupling length $L_c$ for EMD in multimode silica SI PCF with $d = 1$ μm and $d = 2$ μm, for different $(FWHM)_{z=0}$ of the incident beam.

| | $(FWHM)_{z=0=1o}$ | | | $(FWHM)_{z=0=3o}$ | | | $(FWHM)_{z=0=5o}$ | | |
|---|---|---|---|---|---|---|---|---|---|
| | *zSDM* [m] 2-channel | *zSDM* [m] 3-channel | $L_c$ [m] | *zSDM* [m] 2-channel | *zSDM* [m] 3-channel | $L_c$ [m] | *zSDM* [m] 2-channel | *zSDM* [m] 3-channel | $L_c$ [m] |
| $d = 1$ μm | 85 | 35 | 500 | 75 | 30 | 410 | 62 | 25 | 300 |
| $d = 2$ μm | 280 | 80 | 1650 | 260 | 70 | 1520 | 250 | 60 | 1450 |

## Declaration of competing interest

The authors declare that they have no known competing financial interests or personal relationships that could have appeared to influence the work reported in this paper.

## References


[1] D. Richardson, J. Fini, L. Nelson, Space-division multiplexing in optical fibres, Nat. Photonics 7 (2013) 354–362.
[2] Y. Ding, Y. Zou, L. Jin, H. Chen, X. Ma, Fiber-coupled high power laser diode by wavelength multiplexing, in: Proceedings of the Photoelectronic Technology Committee Conferences: Optical Imaging, Remote Sensing, and Laser-Matter Interaction, July-December 2013, SuZhou, China, 2014, p. 91420G.
[3] P.J. Winzer, Optical networking beyond WDM, IEEE Photon. J. 4 (2012) 647–651.
[4] G. Li, N. Bai, N. Zhao, C. Xia, Space-division multiplexing: the next frontier in optical communication, Adv. Opt Photon 6 (2014) 413–487.
[5] J. Pauwels, G. Van der Sande, G. Verschaffelt, Space division multiplexing in standard multi-mode optical fibers based on speckle pattern classification, Sci. Rep. 26 (2019), 17597.
[6] A.K. Vyas, A. Dixit, S. Tiwari, N. Khatri, Investigation of crosstalk and BER in multicore fiber optic transmission link for Space Division Multiplexing, Res. Opt. 8 (2022), 100252.
[7] G. Labroille, B. Denolle, P. Jian, P. Genevaux, N. Treps, J.-F. Morizur, Efficient and mode selective spatial mode multiplexer based on multi-plane light conversion, Opt Express 22 (2014) 15599–15607.
[8] Y. Yan, J. Wang, L. Zhang, J.-Y. Yang, I. Fazal, N. Ahmed, B. Shamee, A. Willner, K. Birnbaum, J. Choi, B. Erkmen, S. Dolinar, New approach for generating and (de)multiplexing OAM modes in a fiber coupler consisting of a central ring and four external cores, in: Optical Communication (ECOC) 2011, 37th European Conference and Exhibition, Sep. 2011, pp. 1–3.
[9] P. St, J. Russell, Photonic crystal fibers, Science 299 (2003) 358–362.
[10] J.C. Knight, Photonic crystal fiber, Nature 424 (14) (2003) 847–851.
[11] D. Gloge, Optical power flow in multimode fibers, Bell Syst. Tech. J. 51 (1972) 1767–1783.
[12] W.A. Gambling, D.N. Payne, H. Matsumura, Mode conversion coefficients in optical fibers, Appl. Opt. 14 (1975) 1538–1542.
[13] M. Rousseau, L. Jeunhomme, Numerical solution of the coupled-power equation in step index optical fibers, IEEE Trans. Microw. Theor. Tech. 25 (1977) 577–585.
[14] A. Djordjevich, S. Savovic, Investigation of mode coupling in step index plastic optical fibers using the power flow equation, IEEE Photon. Technol. Lett. 12 (2000) 1489–1491.
[15] K. Saitoh, M. Koshiba, Empirical relations for simple design of photonic crystal fibers, Opt Express 13 (2005) 267–274.
[16] T.P. Tanaka, S. Yamada, Steady-state characteristics of multimode W-type fibers, Appl. Opt. 18 (1979) 3261–3264.
[17] S. Savovic, A. Djordjevich, A. Simovic, B. Drljaca, Influence of mode coupling on three, four and five spatially multiplexed channels in multimode step-index plastic optical fibers, Opt Laser. Technol. 106 (2018) 18–21.
[18] V.S. Chaudhary, D. Kumar, G.P. Mishra, S. Sharma, S. Kumar, Plasmonic biosensor with gold and titanium dioxide immobilized on photonic crystal fiber for blood composition detection, IEEE Sensor. J. 22 (2022) 8474–8481.
[19] G.P. Mishra, D. Kumar, V.S. Chaudhary, S. Kumar, Design and sensitivity improvement of microstructured-core photonic crystal fiber based sensor for methane and hydrogen fluoride detection, IEEE Sensor. J. 22 (2022) 1265–1272.
[20] V.S. Chaudhary, D. Kumar, S. Kumar, SPR-assisted photonic crystal fiber-based dual-wavelength single polarizing filter with improved performance, IEEE Trans. Plasma Sci. 49 (2021) 3803–3810.